Operational cost analysis of fuel cell electric vehicles under different powertrain-sizing configurations

Yang ZHOU*
FMETO-ST (UMR CNRS 6174), FCLAB (FR CNRS 3539)
Université Bourgogne Franche-Comté, UTBM
Belfort, France
yang.zhou@utbm.fr.

Alexandre RAVEY
FMETO-ST (UMR CNRS 6174), FCLAB (FR CNRS 3539)
Université Bourgogne Franche-Comté, UTBM
Belfort, France
alexandre.ravey@utbm.fr.

Marie-Cécile PERA
FMETO-ST (UMR CNRS 6174), FCLAB (FR CNRS 3539)
Université Bourgogne Franche-Comté, UTBM
Belfort, France
marie-cecile.pera@univ-fcomte.fr.

***Abstract*—This paper presents an operation cost analysis of a fuel cell/battery-based plug-in hybrid electric vehicle under different sizing configurations. Specifically, the size of major energy source (e.g. the fuel cell system) is kept constant while altering the battery capacity. Dynamic programming is then employed to extract the vehicle's operation costs imposed by the consumption of hydrogen and electricity power. Afterwards, a numerical analysis of the impacts on fuel economy, fuel cell durability, battery energy utilization rate is conducted, so as to provide useful guidelines to facilitate the powertrain design and the development of corresponding energy management strategies.**

Keywords—Fuel cell, battery, plug-in hybrid electric vehicle, operation cost, dynamic programming

I. INTRODUCTION

In automotive industry, proton exchange membrane fuel cells (PEMFC) have been gradually considered as the promising solution to mitigate the dependency on traditional fossil fuels due to its zero-emission property and high system efficiency [1]. Nevertheless, the high manufacturing costs and the limited lifetime of PEMFC greatly hinder the massive promotion of fuel cell hybrid electric vehicles (FCHEV).

To enhance the efficiency and durability of FCHEVs, it is necessary to develop reliable control strategies to coordinate the output behaviors of multiple energy sources with respect to the rapid-changing power demand. For example, a multi-mode energy management strategy (EMS) is devised for a FCHEV [2], resulting in the improved fuel economy and fuel cell system (FCS) durability against a single-mode benchmark strategy. However, the number of hydrogen refueling infrastructure is insufficient to meet the present market demand and the hydrogen price is still much higher than electricity price [3]. Hence, plug-in FCHEVs with relatively large battery capacity could be more cost-effective at the current stage. A multi-objective hierarchical EMS is devised for a plug-in FCHEV, which outperforms the charge-depleting/charge-sustaining strategy in terms of energy consumption economy and fuel cell lifetime [4].

In addition, hybrid powertrain design could also generate profound impacts on vehicle's economic and drivability performance. Specifically, for the given vehicular parameters, how to properly determine the sizes of multiple onboard energy sources to meet the propulsion power demand while ensuring the fuel economy and powertrain's durability should be intensively studied. Reference [5] propose an energy-source-sizing method for a 13000 kg fuel cell/battery truck, which can effectively downsize the FCS to 20 kW compared to several tens of kilowatt FCS required by classical solutions. In [6], the sizes of FCS, battery and electric machine in a FCHEV are simultaneously optimized to minimize the vehicle's ownership costs imposed by energy consumption and component sizing.

Despite numerous efforts made in previous works, the mutual affecting mechanism between EMS and powertrain sizing deserves further investigations. To this end, this paper intends to explore the potential impacts on operation cost of a plug-in FCHEV imposed by sizing discrepancies. Specifically, an available sizing configuration (30kW FCS + 6.4kWh Battery) for the Toyota Prius vehicle model (1998 version) in our previous work [2] is deemed as the baseline. Vehicles' degree of hybridization is changed via altering the battery capacity in the baseline configuration. Subsequently, dynamic programming (DP) is adopted to extract the global optimal performance under each sizing-configuration. Afterwards, the impacts on FCS efficiency, durability and battery utilization rate brought by sizing discrepancies are analyzed. Finally, several suggestions to advance the EMS development are put forwarded.

This rest of this paper is organized as follows. Section II introduces the studied vehicle model. The definition of vehicular operational cost and the DP formulation are given in Section III. Section IV presents the numerical cost analysis under different scenarios. The conclusion and future research directions are briefed in Section V.

II. VEHICLE PROPULSION SYSTEM MODELLING

This study focuses on a mid-sized sedan model picked from the vehicular simulator ADVISOR [7], with the main structural parameters given in TABLE I. Note the baseline powertrain sizing configuration is taken from our previous work [2].

A. Powertrain Topology and Vehicle Dynamics

The powertrain topology used in this study is shown in Fig. 1(a), where the PEMFC, attached to the DC bus via a DC/DC converter, and the battery, directly linked to the DC bus, work cooperatively to response the power request from the electric

machine (EM). Under such powertrain, the FCS can charge the battery or directly propel the EM, while the battery can also be recharged through the onboard charger using the grid power.

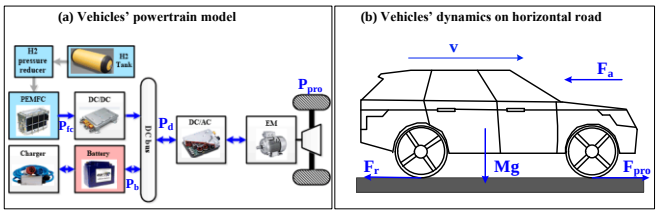

Fig. 1. Representation of (a) powertrain topology and (b) vehicle dynamics.

As shown in Fig. 1(b), the propulsion power P_{pro} needed by vehicle in motion can be denoted as a function of its weight M_v and speed v, as given in (1). Meanwhile, the output power of FCS (P_{FC}) and battery (P_B) work together to meet the DC bus power demand (P_{DC}), as indicated by (2) [5].

$$P_{pro} = v \cdot \left[\overbrace{c_r M_v g \cos(\theta)}^{F_r} + \overbrace{0.5 \rho_{air} S_f c_d v^2}^{F_a} + M_v \dot{v} \right] \quad (1)$$

$$P_{DC} = \frac{P_{pro}}{\eta_{drive} \cdot \eta_{DC/AC} \cdot \eta_{EM}} = P_B + P_{FC} \cdot \eta_{DC/DC} \quad (2)$$

where c_r denotes the rolling resistance coefficient, ρ_{air} the air density, S_f the front surface area, c_d the aerodynamic drag coefficient, g the gravitational acceleration, η_{drive} the driveline efficiency, $\eta_{DC/DC}$, $\eta_{DC/AC}$ the power converters' efficiency and η_{EM} the EM efficiency. Since a horizontal vehicle model is considered in this study, the road slope θ equals to zero.

TABLE I. POWERTRAIN SPECIFICATIONS OF THE STUDIED VEHICLE

Item	Item	Value
Vehicle Structural Parameters	Vehicle mass	1360 kg
	Vehicle front surface	1.746 m^2
	Air density	1.21 kg/m^3
	Aerodynamic coefficient	0.3
	Rolling coefficient	0.0135
	Driveline efficiency	0.91
	Gravitational acceleration	9.81 m/s^2
PEMFC System	Rated power	30 kW
	Maximum efficiency	50.3 %
Battery Pack	Type	Lithium-ion
	Nominal energy capacity	6.4 kWh (Baseline)
Electrical Machine	Maximum power	75 kW
	Maximum torque	271 N·m
	Maximum rotation speed	10000 rpm
Others	DC/DC converter Efficiency	0.90
	DC/AC converter Efficiency	0.95

B. Fuel Cell Model

Proton exchange membrane fuel cell (PEMFC) converts the H2 energy into electricity power via a series of electrochemical reactions, with the H2 mass flow rate denoted as [8]:

$$\dot{M}_{H_2}(t) = \frac{P_{FC}(t)}{\eta_{FCS}(P_{FC}) \cdot LHV} \quad (3)$$

where LHV denotes the lower heating value of H2. P_{FC} is FCS net power, which equals to the difference between the electrical power generated by the fuel cell stack and the power dissipated in auxiliaries [8]. Moreover, η_{FC} is the FCS efficiency. Based on our previous study [2], the relationship between P_{FC} and η_{FCS} of the studied 30 kW FCS is given in Fig. 2, where the highest FCS efficiency ($\eta_{max} = 50.3\%$) occurs when $P_{FC} = P_\eta^{max}$. Besides, $P_{FC} \in [P_\eta^{LOW}, P_\eta^{HIGH}]$ is defined as the high efficiency area of the studied FCS.

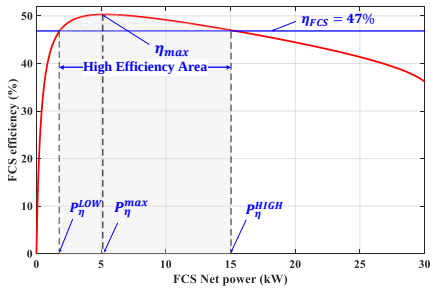

Fig. 2. Efficiency curve of the studied 30kW fuel cell system.

C. Battery Model

As depicted in Fig. 3(a), the internal-resistance (R-int) model is used to characterize the lithium-ion battery. Let I_B denotes the battery current, R_B the internal resistance, Q_B the nominal capacity (Ah), U_{OC} the open-circuit voltage (OCV) and η_B the battery efficiency, the battery SoC and the DC bus voltage (U_{DC}) are determined by:

$$SoC(t) = SoC_0 - \int_0^t \frac{\eta_B \cdot I_B(t)}{Q_B} dt \quad (a)$$

$$I_B = \frac{U_{OC}(SoC) - \sqrt{U_{OC}(SoC)^2 - 4 \cdot R_B(SoC) \cdot P_B}}{2 \cdot R_B(SoC)} \quad (b) \quad (3)$$

$$U_{DC} = U_{OC}(SoC) - I_B \cdot R_B(SoC) \quad (c)$$

where SoC_0 is the initial SoC state. For a single battery cell, its OCV and internal resistance change with SoC. This study adopts a lithium-ion battery model extracted from ADVISOR [7], with its characteristic depicted in Fig. 3(b).

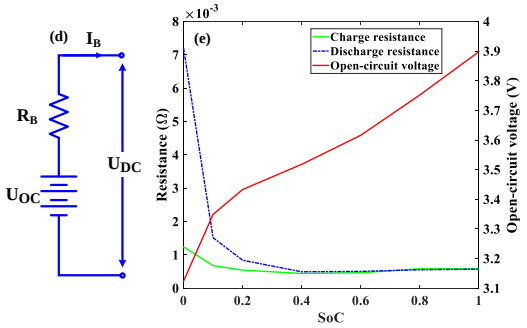

Fig. 3. (a) R-int model and (b) battery cell parameters variation with SoC.

D. Electric Machine Model

From the database of ADVISOR, A 75kW AC electric machine (EM) model is used in this study [7]. The permissible torque and rotation speed range of the selected motor are respectively [-271, 271] N·m and [0, 10000] rpm. Moreover, as shown in Fig. 4, the EM efficiency map is used to compute η_{EM} when the vehicular torque and speed requests are specified.

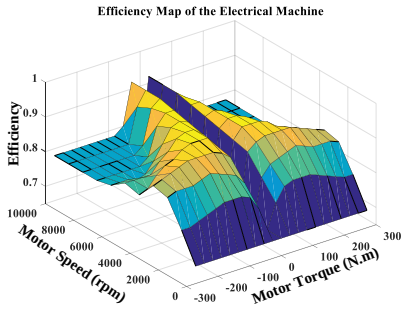

Fig. 4. Efficiency map of the studied electric machine.

III. Operational Cost and Dynamic Programming

This section presents the way of extracting the vehicle's operational cost via dynamic programming (DP).

A. Vehicle Operational Cost Definition

Since both FCS and battery can directly propel the vehicle, the total operational cost (C_{Total}) comprises two parts: the cost owing to hydrogen consumption (C_{H2}) and the cost owing to electricity consumption (C_{elec}), as given by (4). The unit for the cost term is in Chinese yuan in the five-page digest, while an additional case study in Euro will be offered in the final version.

$$\begin{aligned} C_{Total} &= C_{H_2} + C_{elec} \\ &= p_{H_2} \cdot M_{H_2} + p_{elec} \cdot E_{elec} \end{aligned} \tag{4}$$

where p_{H_2} the mainstream H2 price in China at present, p_{elec} the electricity price. Moreover, M_{H_2} denotes the H2 mass consumption (in kg) over a trip, and E_{elec} the electricity power consumption (in kWh), which can be calculated by (5) and (6), respectively, where $\bar{\eta}_B$ denotes the average battery working efficiency. TABLE II lists the values of parameters for operation costs calculation.

$$M_{H_2} = \frac{1}{1000}\int_{t=0}^{N} \frac{P_{FC}(t)}{\eta_{FCS}(P_{FC})\cdot LHV}\,dt \tag{5}$$

$$E_{elec} = \frac{1}{3600\cdot 1000}\int_{t=0}^{N} \frac{P_B(t)}{\bar{\eta}_B}\,dt \tag{6}$$

TABLE II. Value of Parameters for Vehicle Operational Cost

Parameter	Value	Unit	Data source
p_{H_2}	40	yuan/kg	[3]
LHV	120000	J/g	[8]
p_{elec}	1	yuan/kWh	[3]
$\bar{\eta}_B$	0.9	N/A	Assumption

B. Dynamic Programming

To avoid the impacts on vehicle's performance imposed by different control strategies, DP is adopted to find the optimal operation cost under each sizing configuration. Specifically, the global optimization problem is formulated as follows:

$$\min_{\Delta P_{FC}\in\mu_{FC}} \sum_{k=0}^{N-1}\left[p_{H_2}\cdot \dot{M}_{H_2}(k) + p_{elec}\cdot \dot{E}_{elec}(k)\right]\cdot \Delta T$$

$$\text{with} \quad \dot{M}_{H_2}(k) = \frac{1}{1000}\cdot\frac{P_{FC}(k)}{\eta_{FCS}(P_{FC})\cdot LHV} \tag{7}$$

$$\dot{E}_{elec}(k) = \frac{1}{3600\cdot 1000}\cdot\frac{P_B(k)}{\bar{\eta}_B}$$

subject to

$$\begin{cases} 0.2 \le SoC(k) \le 1.0 & (a) \\ 0 \le P_{FC}(k) \le 30\ kW & (b) \\ -1\ kW/s \le \Delta P_{FC}(k) \le 1\ kW/s & (c) \\ -25\ kW \le P_B(k) \le 50\ kW & (d) \\ SoC_0 = SoC_{ini}, P_{FC\_0} = 0\ W & (e) \\ SoC_N = 0.2 & (f) \end{cases} \tag{8}$$

where the FCS power-changing rate ΔP_{FC} is selected as the control variable in DP problem ($\Delta P_{FC}(k) = \frac{P_{FC}(k)-P_{FC}(k-1)}{\Delta T}$). μ_{FC} is the discretized feasible domain for ΔP_{FC}, with the grid resolution of 1 W/s. Constraints (8a) -(8d) respectively specify the operation boundaries for SoC, FC power, FC power transients and battery power. Besides, (8e) indicates the initial states of battery SoC and FC power. Different depth of discharge ($DOD = SoC_0 - SoC_N$) can be realized via using different SoC_{ini}, where SoC_N denotes the final SoC. Constraint (8f) ensures the full depletion of battery energy at the trip end.

To approximate daily driving scenarios, two combined testing cycles are established using different standard driving cycles from ADVISOR [7], including multiple driving patterns (urban/suburban/highway), as depicted in Fig. 5.

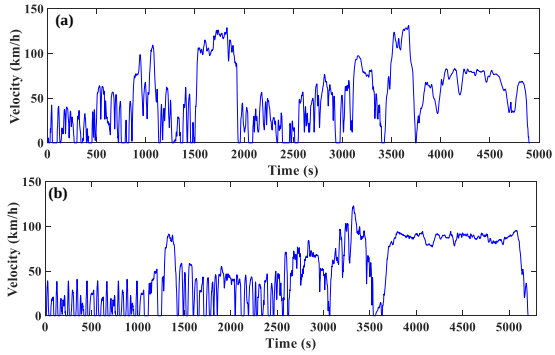

Fig. 5. Speed profiles of (a) testing cycle I (68.5 km) and (b) II (69.7 km).

IV. Vehicle's Operation Cost Under Different Sizing Configurations

A quantitative evaluation on the vehicle's operating costs under different sizes of battery capacity, initial SoC value and driving distance is conducted in this section.

A. Operation Cost Analysis under Different Battery Capacity and Initial SoC

Based on the 30 kW FCS and the battery with different nominal energy capacities (E_B = 1.0 kWh to 15.0 kWh), the DP-based results on vehicle's operation costs over two testing cycles are listed in TABLE III and IV. Two different SoC_{ini} (1.0 and 0.7) are used to respectively simulate a fully charged battery and a non-fully-charged one.

In TABLE III, when SoC_0 = 1.0, if $E_B \ge 12.8$ kWh, the energy stored in the battery pack is sufficient to cover the energy required by the entire driving cycle, where, of course, the operation cost mainly comes from the electricity consumption. In this case, although no FC power is delivered to propel the vehicle, there still exists H2 consumption cost (2.50 yuan). This is because an "always-on" strategy is adopted to limit the times of FCS on-off cycles for better system durability, and thus a

minimal H2 flow rate is needed to supply the compressor and other auxiliaries, with this operational state termed as fuel cell "idle" [9]. If E_B becomes smaller than 12.8 kWh, the FCS gradually becomes the primary energy source for vehicle propulsion, leading to the higher amount of H2 consumption. Consequently, C_{H_2} enlarges 7.56 times (from 2.50 yuan to 21.42 yuan), while C_{Total} increases 85.31% (from 11.98 yuan to 22.20 yuan). The significant cost increment is due to the price of H2 (p_{H_2}) is much higher than the electricity price (p_{elec}).

If the battery pack is not fully charged at the beginning of the trip (SoC_0 = 0.7), the amount of energy stored in the battery is insufficient to cover the energy demand over the entire driving cycle (even with the largest E_B, 15.0 kWh). Compared to the fully charged conditions, this leads to higher C_{H_2} and C_{total} under the same size of battery capacity. With the decrement of E_B, C_{H_2} enlarges 3.61 times (from 4.75 yuan to 21.92 yuan), while C_{Total} increases 71.79% (from 13.08 yuan to 22.47 yuan). In addition, similar results can also be observed on testing cycle II, as shown in TABLE IV.

TABLE III. OPERATION COST COMPARISON WITH DIFFERENT BATTERY CAPACITY UNDER TESTING CYCLE I (68.5 KM)

E_B (kWh)	SoC_0	DoD	C_{H_2} (yuan)	C_{elec} (yuan)	C_{Total} (yuan)	SoC_0	DoD	C_{H_2} (yuan)	C_{elec} (yuan)	C_{Total} (yuan)
15.0	1.0	0.67	2.50	9.48	11.98	0.7	0.50	4.75	8.33	13.08
12.8		0.77	2.50	9.48	11.98		0.50	6.60	7.10	13.70
10.0		0.80	5.69	7.77	13.46		0.50	9.90	5.55	15.45
6.4 (baseline)		0.80	11.63	4.97	16.60		0.50	14.45	3.55	18.00
5.0		0.80	14.09	3.89	17.97		0.50	16.28	2.77	19.06
3.2		0.80	17.29	2.49	19.77		0.50	18.70	1.77	20.47
1.0		0.80	21.42	0.77	22.20		0.50	21.92	0.55	22.47

TABLE IV. OPERATION COST COMPARISON WITH DIFFERENT BATTERY CAPACITY UNDER TESTING CYCLE II (69.7 KM)

E_B (kWh)	SoC_0	DoD	C_{H_2} (yuan)	C_{elec} (yuan)	C_{Total} (yuan)	SoC_0	DoD	C_{H_2} (yuan)	C_{elec} (yuan)	C_{Total} (yuan)
15.0	1.0	0.64	2.64	9.04	11.68	0.7	0.50	4.20	8.33	12.53
12.8		0.74	2.64	9.04	11.68		0.50	5.88	7.12	12.99
10.0		0.80	6.05	7.77	13.83		0.50	9.00	5.55	14.55
6.4 (baseline)		0.80	10.95	4.97	15.92		0.50	13.48	3.55	17.03
5.0		0.80	13.28	3.89	17.16		0.50	15.31	2.77	18.09
3.2		0.80	16.46	2.49	18.95		0.50	17.77	1.77	19.54
1.0		0.80	20.50	0.77	21.27		0.50	20.92	0.55	21.47

Furthermore, the average FCS working efficiency ($\bar{\eta}_{FCS}$) with different battery capacities and initial SoC values are given in Fig. 6. As depicted in Fig. 6(a), when battery is fully charged (SoC_0 = 1.0), zero FCS efficiency occurs when $E_B \geq$ 12.8 kWh. This is because vehicle operates under the pure electric mode with no output electrical power from FCS for vehicle propulsion (FCS idle state).

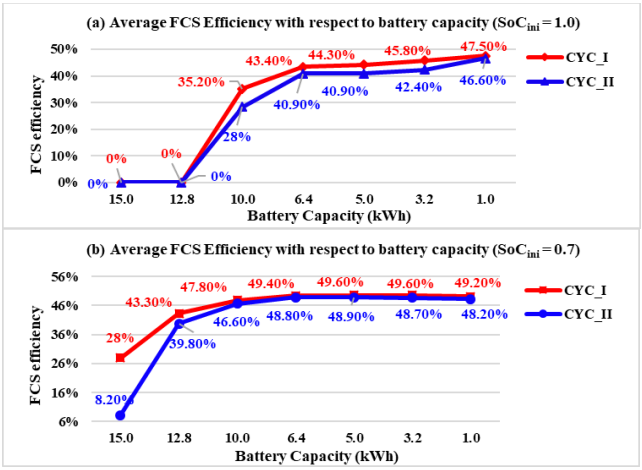

Fig. 6. Average FCS working efficiency with respect to different sizes of battery capacity and different SoC_0 under testing cycle I and II.

Moreover, $\bar{\eta}_{FCS}$ decreases with the increment of E_B and SoC_{ini} (Fig. 6(a) and (b)). This is because a larger capacity and a higher initial SoC imply the larger amount of useful battery energy. When there is sufficient low-cost battery energy for vehicle propulsion, more FCS operating points tend to distribute towards its low power region, thus leading to the decrement of $\bar{\eta}_{FCS}$ since the FCS efficiency drops significantly at low power region (see Fig. 2). Besides, working at extremely low loadings would intensify the (catalyst layer) degradation of a PEMFC [10]. A further fuel cell degradation analysis will be presented in the final version.

B. Operation Cost Analysis under Different Battery Capacity and Driving Distance

With different battery capacities, vehicle's operation cost and FCS working efficiency is evaluated on the concatenated driving cycles (1 to 3 testing cycle I), with the evaluation results summarized in TABLE V. In all simulations, a fully charged battery is used (SoC_0 = 1.0). Moreover, C_{FE} denotes the total cost per kilometer (yuan/km).

If $E_B \leq$ 10.0 kWh, C_{elec} is not affected by the driving distance, meaning the stored battery energy is fully utilized over the trip. If $E_B >$10.0 kWh, battery energy is fully depleted only when the driving distance $\geq$ 137.0 km. Moreover, under the same driving distance, enlarging E_B would contribute to the reduction of C_{FE}, since more low-cost electricity power can be

used for vehicle propulsion. However, with the increment of driving distances, the cost reduction ratios brought by battery capacity enlargement (from 6.4 kWh to 15.0 kWh) are shrinking, namely 25.0% for 68.5 km, 24.1% for 137.5 km and 13.3% for 205.5 km, respectively.

Furthermore, $\bar{\eta}_{FCS}$ grows with the increment of driving distance, especially obvious when $E_B \geq 10.0$ kWh. This is because, for a long-distance trip, the amount of energy required by the driving cycle is much larger than the amount of energy stored in the battery. To bridge such energy gap, larger portion of propulsion power will be supplied by FCS. Therefore, more FCS operating points will move towards its higher power region, leading to the improved $\bar{\eta}_{FCS}$ and better FCS utilization rate. In addition, escaping from the extremely low loadings conditions is beneficial for extending the lifetime of FCS [10].

TABLE V. FUEL ECONOMY COMPARISON WITH DIFFERENT BATTERY CAPACITY AND DIFFERENT DRIVING LENGTH

E_B (kWh)	Distance (km)	C_{H_2} (yuan)	C_{elec} (yuan)	C_{Total} (yuan)	C_{FE} (yuan/km)	$\bar{\eta}_{FCS}$
15.0	68.5	2.50	9.48	11.98	0.18	0%
	137.0	19.15	11.66	30.81	0.22	43.7%
	205.5	41.62	11.66	53.27	0.26	46.5%
12.8	68.5	2.50	9.48	11.98	0.18	0%
	137.0	22.98	9.94	32.92	0.24	45.0%
	205.5	45.54	9.94	55.48	0.27	47.0%
10.0	68.5	5.69	7.77	13.46	0.20	35.2%
	137.0	27.88	7.77	35.65	0.26	46.0%
	205.5	50.70	7.77	58.40	0.28	47.4%
6.4 (baseline)	68.5	11.63	4.97	16.60	0.24	43.4%
	137.0	34.36	4.97	39.33	0.29	46.8%
	205.5	57.25	4.97	62.22	0.30	47.8%

V. CONCULSION

This paper presents an operational cost analysis of a fuel cell/battery-based PHEV under different sizing configurations. The major findings are summarized as below:

On the one hand, with a fixed size of 30 kW FCS, increasing battery capacity would enlarge the amount of available onboard battery energy, indicating a longer all-electric-range. Moreover, since the electricity price is much cheaper than H2 price in some regions of the world (e.g. China), this measure would be helpful to reduce the vehicle's overall operation cost, since more low-cost electricity power can be used for vehicle propulsion, and battery can be recharged by external grid power when trip ends.

On the other hand, increasing battery capacity would reduce the average FCS working efficiency. This is because if there is sufficient low-cost battery energy for vehicle propulsion, the FCS is more likely to work under low power region (or idle condition), meaning the average FCS power level would be reduced, thus leading to the significant drop of FCS efficiency. Moreover, working under extremely low load conditions would also shorten the FCS lifetime, increasing the powertrain maintenance cost.

To sum up, with a 30 kW FCS, if the size of battery capacity in the baseline configuration is slightly increased (e.g. to 10.0 kWh), it would be beneficial for achieving a more balanced performance among the vehicle's operation cost, the FCS efficiency, durability and the battery energy utilization rate.

Future works will develop a co-optimization framework for FCHEVs considering the component degradations, which can simultaneously optimize the sizing configuration and the control policy.

ACKNOWLEDGMENT

This work has gained support from the China Scholarship Council (CSC) and the EIPHI Graduate School (contract "ANR-17-EURE-0002").

REFERENCES

[1] Y. Zhou, A. Ravey, M.C. Péra, A survey on driving prediction techniques for predictive energy management of plug-in hybrid electric vehicles, ***J. Power Sources***, vol. 412, 2019, Pages 480-495.

[2] Y. Zhou, A. Ravey, M.C. Péra, Multi-mode predictive energy management for fuel cell hybrid electric vehicles using Markov driving pattern recognizer, ***Appl. Energy***, vol. 258, 2020, 114057.

[3] X. Wu, X. Hu, X. Yin, Lei Li, Z. Zeng, V. Pickert, Convex programming energy management and components sizing of a plug-in fuel cell urban logistics vehicle, ***J. Power Sources***, Vol. 423, 2019, Pages 358-366,.

[4] Y. Liu, J. Li, Z. Chen, D. Qin, Y. Zhang, Research on a multi-objective hierarchical prediction energy management strategy for range extended fuel cell vehicles, ***J. Power Sources***, vol. 429, 2019, Pages 55-66.

[5] A. Ravey, N. Watrin, B. Blunier, D. Bouquain, A. Miraoui, "Energy-Source-Sizing Methodology for Hybrid Fuel Cell Vehicles Based on Statistical Description of Driving Cycles," in ***IEEE T. Veh. Technol.***, vol. 60, no. 9, pp. 4164-4174, Nov. 2011..

[6] M. Pourabdollah, B. Egardt, N. Murgovski, A. Grauers, "Convex Optimization Methods for Powertrain Sizing of Electrified Vehicles by Using Different Levels of Modeling Details," in ***IEEE T. Veh. Technol.***, vol. 67, no. 3, pp. 1881-1893, March 2018.

[7] ADVISOR. Advanced Vehicle Simulator. http://adv-vehicle-sim.sourceforge.net/.

[8] MC. Péra, D. Hissel, H. Gualous, C. Turpin. Electrochemical Components. ***John Wiley & Sons, Inc***. 2013.

[9] B. Geng, J. K. Mills, D. Sun, "Two-Stage Energy Management Control of Fuel Cell Plug-In Hybrid Electric Vehicles Considering Fuel Cell Longevity," in ***IEEE T. Veh. Technol.***, vol. 61, no. 2, pp. 498-508, Feb. 2012.

[10] T. Fletcher, R. Thring, M. Watkinson, An Energy Management Strategy to concurrently optimise fuel consumption & PEM fuel cell lifetime in a hybrid vehicle, ***Int. J. Hydrogen Energ***., vol. 41, Issue 46, 2016, Pages 21503-21515.